Lessons from the Magellanic System and its modeling

Jianling Wang, Francois Hammer, Yanbin Yang

Monthly Notices of the ROYAL ASTRONOMICAL SOCIETY

MNRAS **515,** 940–952 (2022) https://doi.org/10.1093/mnras/stac1640
Advance Access publication 2022 June 16

Lessons from the Magellanic System and its modeling

Jianling Wang [1]★ Francois Hammer [2]★ and Yanbin Yang [2]

[1]*CAS Key Laboratory of Optical Astronomy, National Astronomical Observatories, Beijing 100101, China*
[2]*GEPI, Observatoire de Paris, CNRS, Place Jules Janssen, F-92195 Meudon, France*

Accepted 2022 June 8. Received 2022 April 23; in original form 2021 December 15

ABSTRACT

The prominent Magellanic Stream that dominates the H I sky provides a tantalizing number of observations that potentially constrains the Magellanic Clouds and the Milky Way (MW) outskirts. Here we show that the 'ram-pressure plus collision' model naturally explain these properties, and is able to predict some of the most recent observations made after the model was made. These include the complexity of the stellar populations in the Magellanic Bridge, for which kinematics, ages, and distances are well measured, and the Northern Tidal Arm, for which the model predicts its formation from the MW tidal forces. It appears that this over-constrained model provides a good path to investigate the Stream properties. This contrasts with tidal models that reproduce only half of the Stream's main properties, in particular a tidal tail cannot reproduce the observed inter-twisted filaments, and its gas content is not sufficiently massive to provide the large amount of H I and H II gas associated to the Stream. Despite the efforts made to reproduce the large amounts of gas brought by the Clouds, it seems that no viable solution for the tidal model could be foreseen. Since the 'ram-pressure plus collision' model has not succeeded for a Large Magellanic Cloud mass above 2×10^{10} $M_\odot$, we conjecture that a low mass is required to form the Stream.

Key words: Galaxy: halo – Galaxy: structure – galaxies: evolution – Galaxies: interactions – Galaxies: Magellanic Clouds.

1 INTRODUCTION

Together, the Magellanic Stream (MS) and Leading Arm (LA) subtend an angle of 230°, making it the second most prominent neutral hydrogen structure dominating the sky, after the Milky Way (MW). The MS has been identified to be anchored to the Magellanic Clouds in 1974 by Mathewson, Cleary & Murray (1974), though the nature of its formation was considered still unknown in 2012 (Mathewson 2012). *HST* proper motion measurements of the Magellanic Clouds by (Kallivayalil et al. 2006; Piatek, Pryor & Olszewski 2008; Kallivayalil et al. 2013) indicate that the Clouds are presently moving at high velocities, and are consistent with a first passage about the Galaxy (Besla et al. 2007). In such a frame, modeling of the MS has followed two very different and mutually exclusive schemes, since either it can be a tidal tail (and references therein Besla et al. 2012), or it can be made by one or two ram-pressure tails (Mastropietro 2010; Hammer et al. 2015).

Today the most influential tidal model of the MS is that of Besla et al. (2012), for which the MS is a gigantic tidal tail extracted from the Small Magellanic Cloud (SMC) by the tidal effect of the Large Magellanic Cloud (LMC) during a close interaction 1.2–2 Gyr ago. The SMC is further assumed to be a long-lived satellite of the LMC, which imposes a very large mass for the latter, in excess of 10^{11} $M_\odot$ (Kallivayalil et al. 2013). The strengths of the Besla et al. (2012) model are their predictions of the MS length, of the 6D space-velocity phase of the Clouds, and that it predicts at least one arm of the LA.

The major limitations of the Besla et al. (2012) tidal model include (i) that only a small fraction, few per cent, of the MS gas is reproduced, and no ionized gas while it is the prominent component of the MS (Fox et al. 2014), (ii) the stream is made of two filaments, with kinematic and chemical analyses indicating that gas from both the LMC and SMC is present, and (iii) the absence of stars in the Stream observed so far.[1] Each of these limitations appear to be a showstopper for the tidal model of the MS.

The Besla et al. (2012) model is also limited because it neglects the presence of a coronal phase in the MW halo, while the presence of a multiphase circumgalactic medium has been evidenced by many means (X-rays: Miller & Bregman 2013; Faerman, Sternberg & McKee 2017; Bregman et al. 2018; QSO absorption lines: Fox et al. 2014; Zheng et al. 2015, 2019; Richter et al. 2017; LMC shrunk gas disc: Nidever 2014; high velocity cloud dissociation: Kalberla & Haud 2006). More recent realizations of the tidal model have introduced the MW coronal phase together with that of a putative LMC corona (Lucchini et al. 2020; Lucchini, D'Onghia & Fox 2021).

Compared to tidal models, the 'ram-pressure plus collision' model (Hammer et al. 2015; Wang et al. 2019) appears much more advanced since it reproduces in details many known properties of the MS, as well as some qualitative. In this model the LA is produced by the leading passages of gas-rich dwarfs assumed to be progenitors of

★ E-mail: wjianl@bao.ac.cn (JW); francois.hammer@obspm.fr (FH)

[1]Besla, Hernquist & Loeb (2013) argued that the absence of stars could be due to their expected very low surface brightness, especially if only few stars were extracted from a very gas-rich SMC. Zaritsky et al. (2020) recently claimed a positive detection of stars near the MS tip end, which is at odd with the Besla et al. (2013)'s argument, since the MS furthest part is likely at its tip end. However, this detection of MS stars needs confirmation, because they are offset from the H I gas stream and their distance are much lower than model's expectations.

present-day MW dwarfs (see also Tepper-García et al. 2019). This hypothesis has been also adopted by the most recent tidal model of the MS (Lucchini et al. 2021), and is further supported by the MW dwarf high energies and angular momenta, suggesting also a recent passage for them (Hammer et al. 2021). By construction, the 'ram-pressure plus collision' model reproduces the dual filamentary structures, which are two ram-pressure tails attached to each Clouds, the whole H I MS shape and gas mass and its radial velocity (Hammer et al. 2015). The recent collision between the Clouds explains the Magellanic Bridge (MB), leading to Cloud proper motions consistent with the observed values. It also reproduces the velocity field of the LMC and the gigantic, 30 kpc-long, structure along the line of sight of the SMC young stars (Ripepi et al. 2017; Wang et al. 2019), which both are due to the recent, 300 Myr old, collision between the gas-rich Clouds. Moreover, the MS ionized gas deposited during the MC motions in the MW halo is coming from the H I gas of the Clouds, which has been extracted by ram-pressure, and then ionized by the hot corona of the MW (Wang et al. 2019).

However and quite surprisingly, the 'ram-pressure plus collision' model does not assume a dark matter component for both Clouds, while it naturally reproduces the MS in details without fine-tuning. It even constrains the LMC mass to be smaller than 2×10^{10} $M_{\odot}$, because otherwise it would not let sufficient expelled gas to make the mass of the H I and especially that of the H II MS. This may come at odd with LMC mass estimates based on the interaction between the MW and the LMC (Erkal et al. 2019, 2021; Conroy et al. 2021; Vasiliev, Belokurov & Erkal 2021).

In this paper we aim at testing the 'ram-pressure plus collision' model by considering the most recent and new constraints on the Magellanic System. The tests include the morphological-age-kinematics distribution of stars in the MB, and the morphological and kinematic behaviour of the faint Northern Tidal Arm (NTA), which stretch an angle of 12.5°. In principle, the tantalizing number of observations that are reproduced makes this model over-constrained and hence, able to be predictive. The paper is organized as it follows. In Section 2, we describe the observational properties of two populations identified in the MB region, the 'ram-pressure plus collision' model from Wang et al. (2019), comparison between MB stellar populations and predictions from the simulations,as well as an interpretation of their origin. In Section 3, we compare the Gaia results for the NTA with our simulation model predictions. In Section 4, we discuss the advantages and inconveniences of the different Magellanic System modeling, and then conclude in Section 5.

2 THE TWO STELLAR POPULATIONS IN THE MB

2.1 Additional constraints from the bridge

In the MB region, the neutral gas bridge has been well identified by H I observations (Nidever et al. 2010), which well elucidate the mutual interaction between MCs. A population of young stars in the Bridge has been also identified by various observations (Irwin, Kunkel & Demers 1985; Demers & Battinelli 1998), and their strong correlation with the MB neutral gas indicates that they likely result from *in situ* star-formation during the recent MC interaction (Skowron et al. 2014; Belokurov et al. 2017).

Besides young stars in the Bridge region, older age RGB (red giant branch) stars have been also discovered by Bagheri, Cioni & Napiwotzki (2013), Noël et al. (2013), and Skowron et al. (2014) identified the presence of red clump stars as well. These older age stars are either distributed with a large scatter in the Bridge region or in front of the gas Bridge region with respect to the motion direction (see also Belokurov et al. 2017).

Recent observations of the MB have confirmed stellar populations with ages ranging from Young Main Sequence stars and old ancient RR Lyrae (Belokurov et al. 2017). Based on star formation and orbital past histories of the Clouds, the MB has been formed ∼200–300 Myr ago (Casetti-Dinescu et al. 2012; Hammer et al. 2015). Thanks to the *Gaia* precise proper motion data, stellar tangential motions have been measured in the MB region, revealing that stars in the MB are leaving SMC towards the LMC (Belokurov et al. 2017; Gaia Collaboration 2021; Omkumar et al. 2021; Zivick et al. 2019; Schmidt et al. 2020). It suggests that they have been stripped from the SMC due to the LMC tidal force. By using the red clump (RC) as standard candle, Nidever et al. (2013) found that there are two stellar populations with different brightnesses within the MB, which has been recently confirmed by Omkumar et al. (2021). With *Gaia* DR2 data, Omkumar et al. (2021) found that the bright star population at the SMC distance has a larger tangential velocity than the fainter, more distant population. This observation may provide a useful constraint for models to simulate the formation of Magellanic System.

2.2 Comparison between simulated data and observations

2.2.1 The ram-pressure plus collision model

Wang et al. (2019) adapted a 'ram-pressure plus collision' model to reproduce the MS and MCs formation using the state-of-the-art software GIZMO (Hopkins 2015). In this model the MS is formed by an interaction between MCs and ram-pressure exerted by the MW hot corona. It leads to dual H I streams behind each MCs, and explains the kinematics and the mass of the huge amount of ionized gas kinematically coupled with the MS. Besides this, the strong interaction between MCs tidally reshapes SMC to a very elongated structure.

In the model of Wang et al. (2019), the stellar distribution of SMC consists of a disc and a spheroid components. The stellar disc is an exponential distribution with scalelength 1.5 kpc, and the spheroid component follows the profile of Dehnen (1993) with $\gamma = 0$, which has a core in the centre with half mass radius 5.8 kpc. The stellar disc represents the young star population observed in the SMC, while the extended spheroid component is motivated by the spheroidal distribution of ancient RR Lyrae stars observed around the SMC (Ripepi et al. 2017). This model of the SMC have been shown to reproduce well the very extended cylindrical structure with line-of-sight distance around 30 kpc for young stars, as well as the nearly spheroidal distribution of RR Lyrae stars (Scowcroft et al. 2016; Ripepi et al. 2017; Wang et al. 2019). Wang et al. (2019) discussed all details for the initial conditions and modeling.

To compare the 3D morphology of MCs with RR Lyrae data and Classic Cepheid observed in Ripepi et al. (2017), Wang et al. (2019) have randomly selected particles to match the numbers to the observed stars, and to match the observed region. This renders it difficult to distinguish the faint features around MCs, especially in the MB region as shown in fig. 7 of Wang et al. (2019).

Here, to have a view of the whole particle distribution in 3D space, we now show in Fig. 1 the simulated MCs particles distribution with all of particles used in our simulation model of Wang et al. (2019). The green colour dots indicate the LMC particles, while the cyan colour dots represent the SMC. In this figure, particles distribute over a much larger region than in fig. 7 of Wang et al. (2019), which illustrates well that the MB is connecting both MCs.

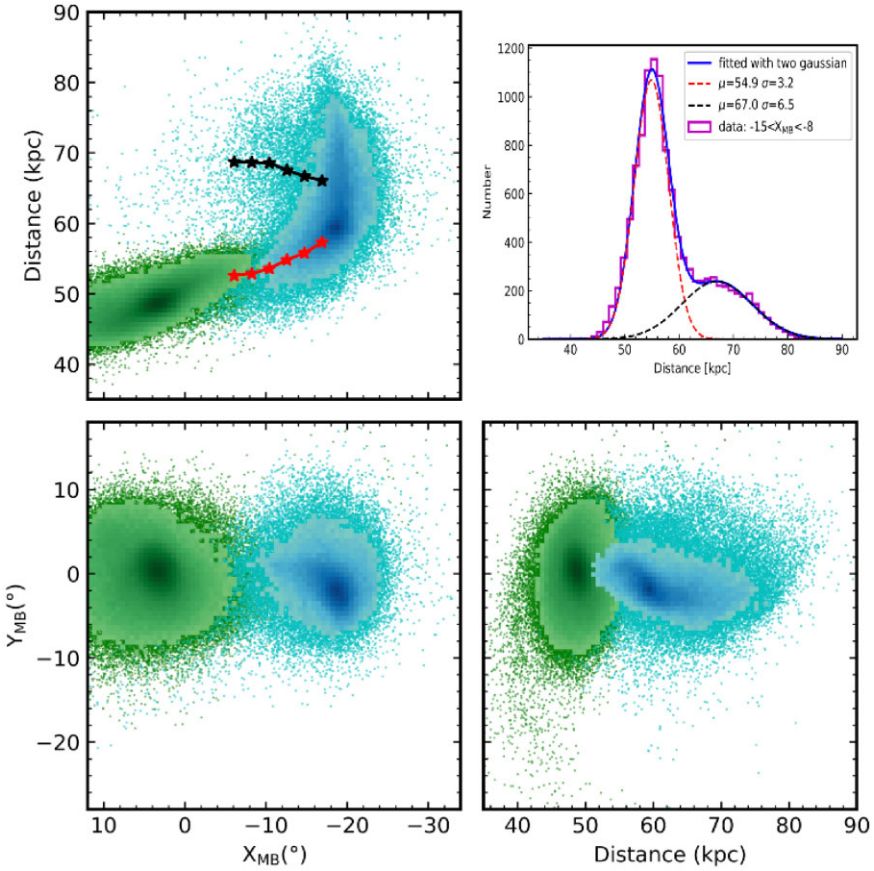

Figure 1. Simulated particles distributions of LMC and SMC in MB coordinates (Belokurov et al. 2017; bottom left), or MB longitude/latitude versus distance (bottom right and top left, respectively). Greens (cyan) points are particles from LMC (SMC). In the top left-hand panel, the red and black big stars indicates the mean distance values along MB longitude for the background and foreground population, which are separated at 60 kpc. The top right-hand panel indicates the distance distribution for stars within the Bridge region, to which are overplotted two Gaussian functions fitted to this distribution and the fitted results are labeled on this panel.

2.2.2 *Two stellar populations at different distances in the Bridge*

Fig. 1 presents the whole star particle distribution in MB coordinates (Belokurov et al. 2017) and also identifies their distances. In Fig. 1 all particles are shown and their colours identify whether they belong to the LMC (green) or to the SMC (cyan). In the X_{MB} versus distance panel (top left-hand panel), there is a tidal bridge (red dots) connecting LMC to SMC with distance varying from $\sim$ 65 kpc (SMC) to $\sim$ 50 kpc (LMC), which forms the stellar MB. Behind the MB, there are particles of SMC distributed from 60 to 80 kpc, which originated from the SMC after tidal interaction with LMC. The MB and background populations of SMC are clearly separated in distance.

In the top right-hand panel of Fig. 1 the distance distribution of particles within $-15^\circ \lesssim X_{MB} \lesssim -8^\circ$ are shown with a magenta line. There are two populations with different distances distribution. Two Gaussian functions (red dashed and black dashed lines) are used to fit these two populations, and the results for the mean and standard deviation of distance are labeled on the top right of this panel. The two populations are clearly located at two different distances, one at $\sim$55 kpc that delineates the mean value of the MB, the other one having a broader distance distribution with a mean value of $\sim$67 kpc. The two populations are well separated at $\sim$60 kpc.

Omkumar et al. (2021) used RC stars to trace distance and found that the stellar population in the east part of SMC have two different populations at different distances. To better compare with observation data, we fitted two Gaussian functions with distance distribution for different MB longitude bins. The fitted results are shown in the Fig. A1 of Appendix. All of the distance distributions at different bins are well fitted with two Gaussian functions. We note that the foreground population between 50 and 60 kpc is the dominant component for all the distribution bins, while it is less prominent in the observation (see fig. 4 of Omkumar et al. 2021). This indicates that the interaction between LMC and SMC is so strong in the simulation that too many particles are tidally stripped from the SMC. A fine tuning model parameters is needed to reduce this component to match with observation. For example, this can be done by either increasing the pericentre to decrease the tidal force, or by decreasing the size or the mass of the SMC disc component, or to change the SMC inclination angle relatively to the orbital plan in order to decrease resonance.

Fig. 2 compares the distance variation at different SMC radii for the two components, allowing to compare observation data and simulation results. The observed data are shown in green (bright RC population) and cyan (faint RC population), with solid squares for the north-east and open squares for the south-east. The two Gaussian fitted results to the simulation data are shown with red (foreground population) and black (background population) colours. The simulated foreground population follow the trends that its distance decreases with increasing SMC radius, which matches with

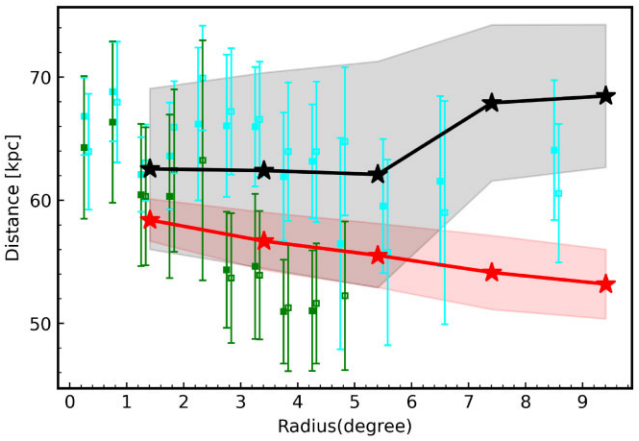

Figure 2. Comparing relations of distances varied with radius to the SMC between observation and simulations. Green and cyan colour indicate bright and faint population of RC from Omkumar et al. (2021) for north-east (solid square) and south-east region (open square). Simulation data from Model-52 are shown by red and red stars, and the grey and pink region shown the 1σ distance scatter.

the observed bright RC (green square) population. The background population in the simulation has a nearly flat distance distribution at radii less than $\lesssim 7^{\circ}$, and the distance increases at radii $\gtrsim 7^{\circ}$, which is roughly similar to the faint RC population.

In our model, the progenitor of SMC consists of a disc and a spheroid component (Wang et al. 2019). In Fig. 3 the spheroid (left-hand panels) and disc (right-hand panels) components of SMC are separated and shown in the MB coordinates or longitude/latitude versus distance. The background population are mainly coming from the spheroidal component, while the foreground component includes contributions from both the spheroid and the disc component.

2.2.3 *Kinematic features for the two populations*

Using *Gaia* DR2, Omkumar et al. (2021) studied the proper motions of these two populations, and found two populations with different kinematics. They identified the proper motions of the two populations in both directions (μ_α, μ_δ) as well as their variations against the SMC radius.

Left-hand and middle panels of Fig. 4 show the relative proper motions variation of the two populations with respected to SMC as function of radius to SMC. The background (faint) and foreground (bright) RC are shown with black and red squares, while the modelled background and foreground are shown with black and red solid lines. The background (faint) RC component has been argued to belong to the main body of SMC (Omkumar et al. 2021; James et al. 2021), but this has to be clarified. This is because there are systematic differences ($\sim$0.16 mas yr^{-1}) of μ_α and μ_δ near the central regions (see black squares at zero radius in left-hand and middle panels of Fig. 4). The modeled proper motions reproduce qualitatively the observations by many aspects, including the variations of proper motions in both directions with the SMC radius. Both observations and simulations show that the foreground population has larger μ_α than the background population (left-hand panel), and that this relation is inverted in the μ_δ (middle panel). The right-hand panel of Fig. 4 shows the radial velocity as function of radius for the model. Both the background and foreground population shows increasing velocity with increasing radius, namely it increases toward to LMC. The background population have higher radial velocity than foreground population. With *Gaia* EDR3 and collected radial velocity data from literature, James et al. (2021) identified two radial velocity components in the eastern region of SMC for the RGB stars with velocity difference by $\sim$35–45 km s^{-1}. The higher (lower) radial velocity component has proper motions consistent with the background (foreground) RC population. This suggests that the lower velocity component belongs to the same substructure than the foreground population, and the higher velocity

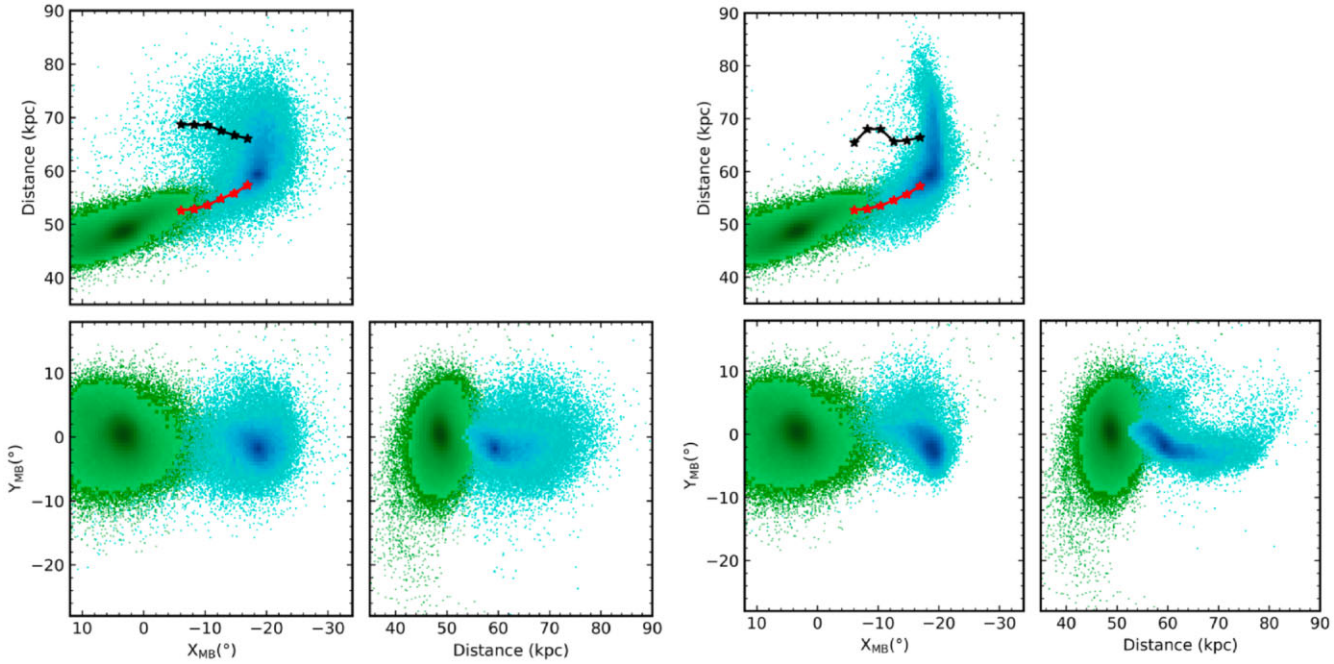

Figure 3. Particles distributions in the MB longitude, latitude, and distance space. The left-hand panels show spheroid component of SMC and the right-hand panels present the disc component of SMC. The black and red stars indicate the mean distance along with the MB longitude for stars separated at 60 kpc.

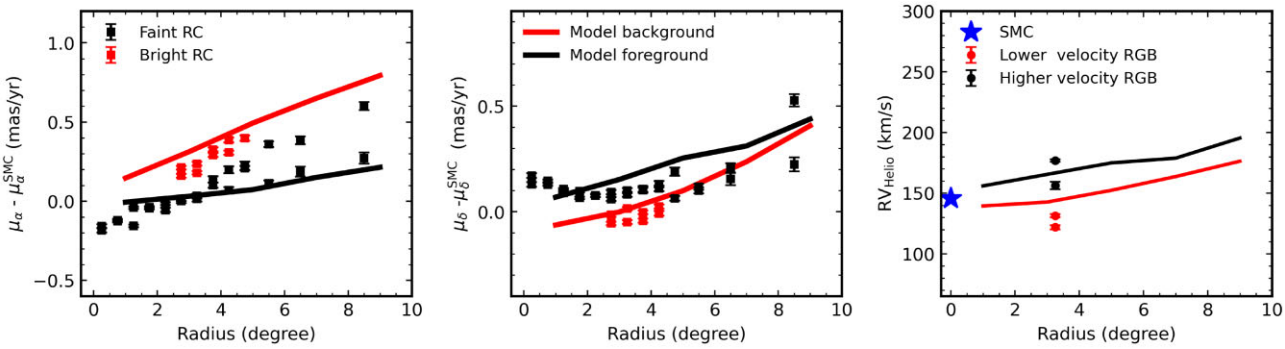

Figure 4. The relative variation of proper motions with respect to that of SMC as function of radius to SMC are shown in left-hand and middle panels, and the right-hand panel shows the radial velocity variation as function of radii to SMC. The observed proper motions and radial velocity of SMC are from Zivick et al. (2018). The proper motion of faint (black square) and bright (red square) RC in the left-hand and middle panel are from Omkumar et al. (2021). The radial velocity of the lower (red circles) and higher (black circles) velocity RGB stars are from James et al. (2021), which are corresponds to foreground components and main body of SMC.

component corresponds to the main body of SMC as well as the background component. In the right-hand panel of Fig. 4 the two radial velocity components of RGB from James et al. (2021) are shown by black and red circles. Even though the difference of radial velocity between background and foreground in our model is smaller than that observed, our model correctly predicts that the foreground component has a lower velocity than that in thebackground.

Gaia Collaboration (2021) have confirmed the above observational results with *Gaia* EDR3 data, showing that there are both young and old stellar bridge having both their proper motions towards the LMC. To have a comparison, we selected young population as required stars with age smaller than 150 Myr, and old stars with age larger than 2 Gyr which are corresponding to the intermediate-old red clump population used in Gaia Collaboration (2021). The top left-hand panel of Fig. 5 shows the young stars distribution on the sky, and the blue arrows indicate the proper motion vector with respect to SMC. In the top right-hand panel of Fig. 5 the old population shows a bridge connection between the LMC and the SMC, which has proper motions similar to that of young stars moving from the two Clouds. For comparison, data from *Gaia* EDR3 are shown in the bottom panels of Fig. 5 from Gaia Collaboration (2021). Both young and old population in the Bridge region share similar motion properties for both observations and model, in particular the Bridge star motions towards the LMC. Only qualitative comparison is feasible because there is no available length scale for the proper motion vectors in the observation data from Gaia Collaboration (2021). Even though these qualitative comparisons indicate the model reproduce well the observation proper motions, there is one difference between the model and data. For example, the proper motions of outskirts of the LMC have a bottom-right bulk motion in the model but a bottom left pattern in the data.

3 THE NORTHERN TIDAL ARM

In this section we examine the giant tidal arm associated with LMC, and its observational properties are reproduced by the Wang et al. (2019) model.

3.1 The general properties of observed and modeled Northern Tidal Arm

By using the first year Dark Energy Survey data, Mackey et al. (2016) identified the NTA, which emanates from the edge of LMC, and stretches more than 12.5°. This feature has been confirmed by further studies (Mackey et al. 2018; Belokurov & Erkal 2019). The stellar population of the NTA matches well that of LMC, which is predominantly old with $[Fe/H] \sim -1$. This indicates a LMC origin for the NTA. *Gaia* EDR3 provides deep astrometric data, and in particular, proper motions may provide important constraints about the NTA origin.

Gaia Collaboration (2021) confirm this NTA feature and found that it stretches to more than 20°, with NTA stars showing motions towards the LMC (see their fig. 17). To compare with the *Gaia* data, we project our simulation data (see the panel (b) of Fig. 6) to the same frame as Gaia Collaboration (2021). Simulations predict a north giant stream starting from the LMC edge, which match well with the NTA, though it stretches a larger angle, $\sim 60°$.

Since the discovery of NTA, several simulation models have been run to explore the origin of NTA (Mackey et al. 2016; Belokurov & Erkal 2019; Cullinane et al. 2022a). As pointed out by Gatto et al. (2022) they only produced a more diffuse twisted stream. In the panel d of Fig. 6 we show the surface number density distribution of our simulation model. Our model can produce a straight stream that resembles the NTA. The NTA is thin in particular at the tip, but at the edge of LMC the simulated NTA are thick, which are likely associated to other substructures (see discussion in next section).

Panel (a) of Fig. 6 shows the distance versus the longitude distribution. The simulated NTA shows a gradient in distance, which decreases from the edge of LMC to ∼38 kpc at 30° away from the LMC, and then increases to ∼56 kpc at ∼55° away from LMC. It confirms that the NTA originates from the LMC. We note that the recent observation from Magellanic Edges Survey (MagES Cullinane et al. 2020, 2022a) have confirmed an LMC origin for the NTA on the basis of its geometry, metallicity, and kinematics.

In the simulation, the interaction between the Clouds triggers instabilities of LMC disc, and then the disturbed LMC disc further suffers the strong MW gravity tidal field that forms a tidal arm and stretches it along when the LMC falls into the MW. This explains well why NTA and LMC stellar population are so similar. The simulation thus predicts that there may be a much longer NTA at lower surface brightnesses, which needs to be confirmed by deeper observations.

3.2 Comparing the morphology of NTA and NES with observation

Fig. 7 give a close comparison morphology of substructures in the periphery of LMC. The left-hand panel shows the faint features presented in Gaia Collaboration (2021) with *GAIA* EDR3, in which

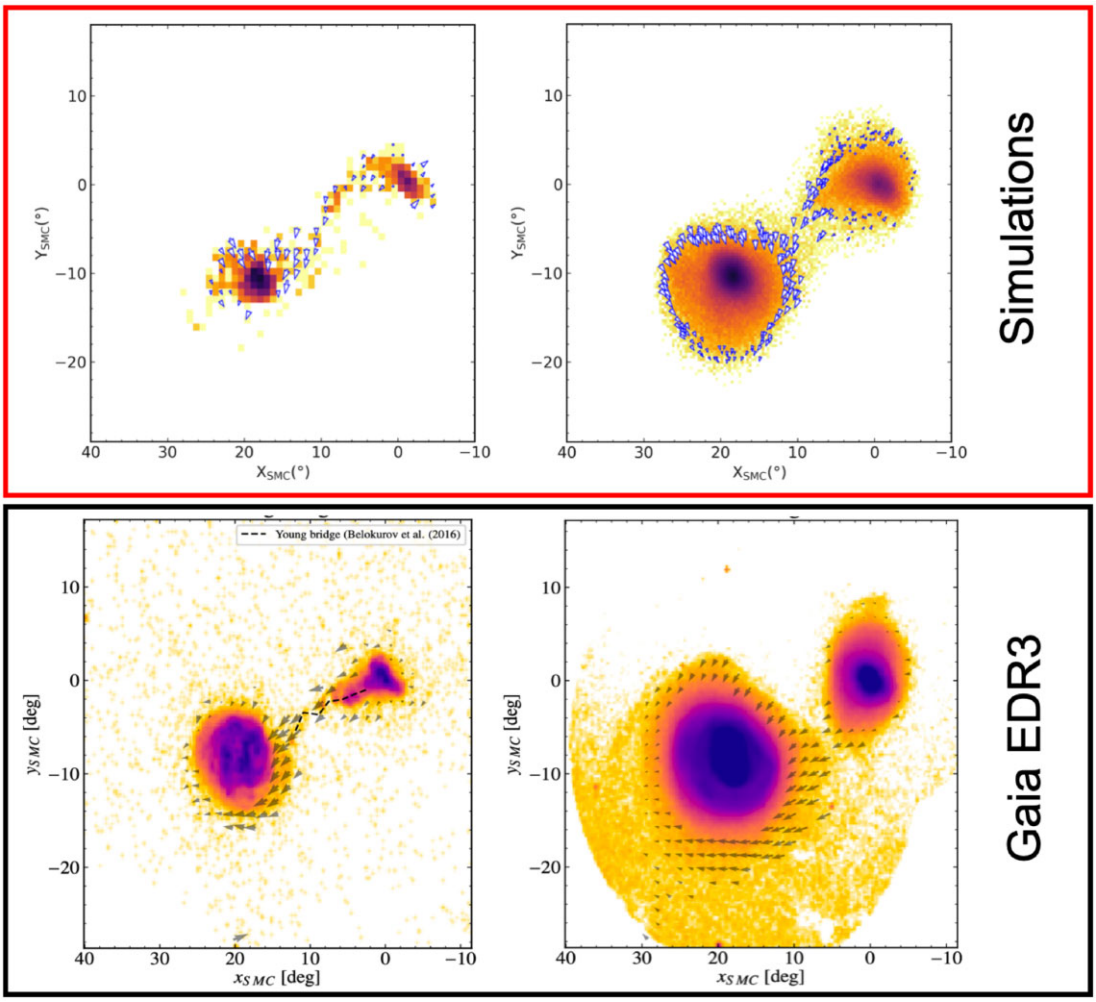

Figure 5. Comparing the young and old population bridge between simulation model and *Gaia* EDR3 data. Vector field are overlapped on the density maps for young stars (left-hand panels) and old stars (right-hand panels). The coordinates has been centred on SMC for comparison with new results from *Gaia* EDR3 (Gaia Collaboration 2021). There is clearly young star bridge connecting LMC and SMC, and moving toward to the LMC, which are consistent with the *Gaia* EDR3 results (bottom panel) for both density map and velocity vector (Gaia Collaboration 2021). There is also old stellar bridge for the observation and simulation results. Since there are no quantitative length scale of proper motion vector available for the observation data from Gaia Collaboration (2021), the length scale of arrows are not matched between observation and model.

the NTA is clearly identified as well as several other substructures indicated by arrows, such as ESS (El Youssoufi et al. 2021). Recently, using a Gaussian Mixture Model to a strictly selected sample of Magellanic System, Gatto et al. (2022) confirmed these substructures, e.g. NTA (red polygon in the right-hand panel of Fig. 7) and ESS (magenta rectangle in the right-hand panel of Fig. 7). In the meanwhile, they also find a new diffuse sub-structure protruding from the outer LMC disc, which extends to more than 20° from the centre of LMC. The new feature is named NES and indicated by a blue polygon in the right-hand panel of Fig. 7.

The middle panel of Fig. 7 shows our model, which predicts both the NTA and the NES. Besides these two structures, in the eastern part of LMC there is substructure which could be associated with ESS. In the bottom left-hand panel of Fig. 6, there are many particles along the NTA in the eastern of LMC, which have the same origin as NTA and are induced by Galactic tides on the LMC. Therefore, the Wang et al. (2019) reproduces NTA, NES, and ESS. Future observations to measure the metallicity of NES and ESS are needed to compare with NTA and verify their origin.

3.3 The distance to NTA

Cullinane et al. (2022a) using data from Magellanic Edges Survey (MagES; Cullinane et al. 2020) and *Gaia* EDR3 have studied the kinematic, metallicity and distance for the NTA. Their fields cover to ∼20° along NTA. They found that the NTA is near the plane of the LMC disc, with an inclination $i = 34°$ and an orientation $\Omega = 139.1°$ (van der Marel & Kallivayalil 2014). Fig. 8 shows the line of sight distance for our model, in which coloured circles indicate an inclined disc with a geometry following van der Marel & Kallivayalil (2014). Our modeled NTA follows well this inclined disc within ∼20°, which is consistent with measurements by Cullinane et al. (2022a).

Fig. 8 shows a gradient of distance in our modeled SMC from the eastern to the western part of the SMC, with the western part (see red colour on the right) at more far distance than the eastern part (see green colour on the left of the SMC). In the observation, there is indeed a distance gradient identified with different tracers. Muraveva et al. (2018) used 2997 RR Lyrae stars to study the 3D structure of SMC. They found that the line-of-sight depth of SMC is in the range 1–10 kpc, and the eastern part of the SMC is located closer to us

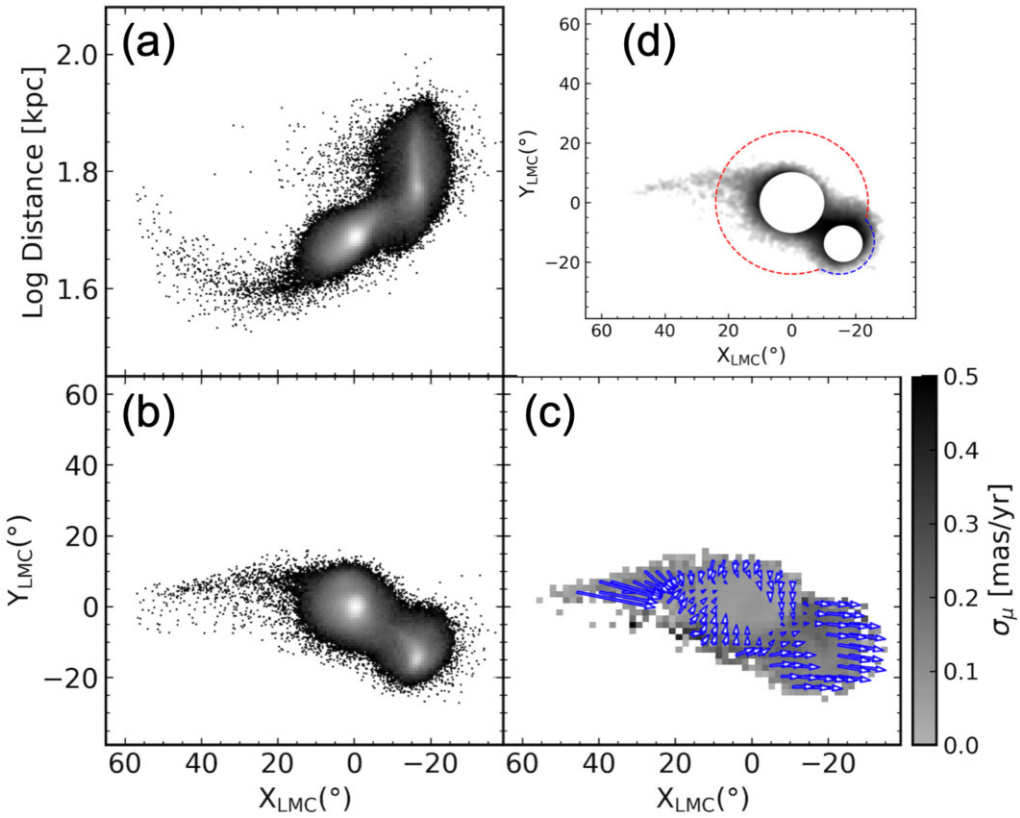

Figure 6. The distribution of modeled MCs in the sky and distance maps. Panel (a): Particles distance distribution along X_{LMC}. Panel (b): Particle distribution in the sky with orthographic projection (see the defination in Gaia Collaboration 2021). Panel (c): Particle distribution with colour indicates proper motion dispersion comparing with *Gaia* data (Gaia Collaboration 2021), and blue arrows show the proper motion vectors. Panel (d): Number density distribution of simulation model. The red and blue dashed line indicate the selection region with Gaia EDR3 in Gaia Collaboration (2021).

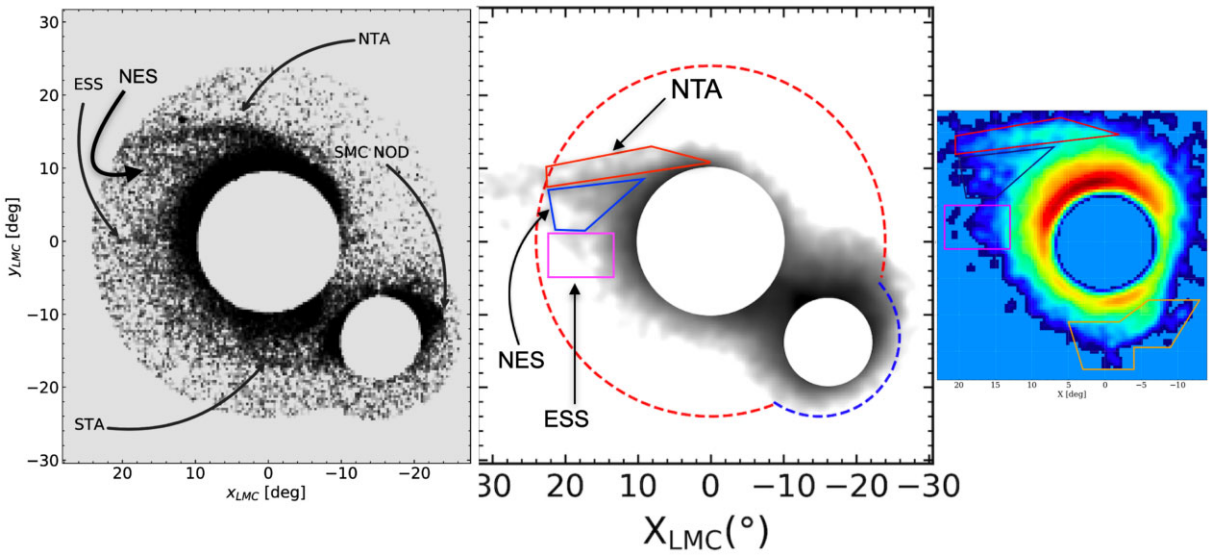

Figure 7. Comparing the morphology of MCs with Gaia EDR3 data. The left-hand panel is from Gaia Collaboration (2021), the middle panel shows the Wang et al. (2019) model, and the right-hand panel is from Gatto et al. (2022) using Gaia EDR3 data with a Gaussian Mixture Model to a sample of strictly selected candidate members of the Magellanic System. In the middle panel, the red and blue dashed line indicate the sample selection region for Gaia data (Gaia Collaboration 2021). In the right-hand panel, the coloured polygon regions indicate different substructures associated with LMC detected by Gatto et al. (2022). The red, blue, and magenta polygon regions on right-hand panelindicate the NTA, North-Eastern Structure (NES), and Eastern Substructure (ESS), which are placed on the middle panel with corresponding position.

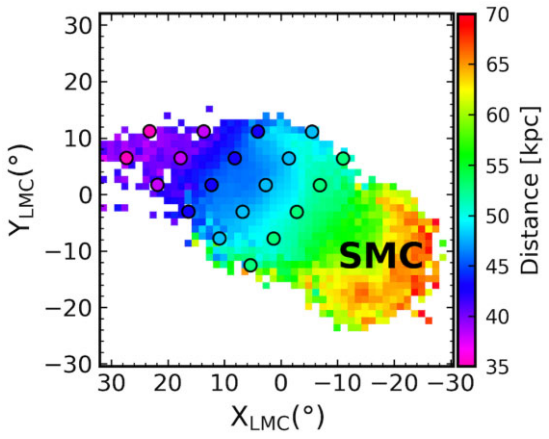

Figure 8. The distribution of the line-of-sight distance for our modelled MCs, and the coloured circles show the distances for a disc with inclination $i = 34°$ and orientation of 139.1° following van der Marel & Kallivayalil (2014). By examining the distances for a few observed fields associated with NTA with red clump stars, Cullinane et al. (2022a) found that the distance distribution of NTA follow the disc geometry of van der Marel & Kallivayalil (2014) very well within ∼20°.

than that of the western part. Grady, Belokurov & Evans (2021) used Gaia DR2 RR Lyrae to trace the 3D distribution of MCs, and they arrived to the same conclusion, i.e. the eastern portion of SMC lies at closer distance. Scowcroft et al. (2016) used classical Cepheids to study the 3D structure of the SMC, and they found that the eastern side is up to 20 kpc closer than its western side. The different distance gradient depends on the different stellar populations, which reflects the different morphologies and line-of-sight distributions (Ripepi et al. 2017). Even though detailed comparison of the depth distribution for SMC between observation and our model will require detailed stellar population modeling and sample selection, the Wang et al. model predicts and reproduces the existence of this distance gradient from eastern to western part of SMC.

3.4 The kinematics of NTA

Fig. 9 compares the proper motions from Gaia EDR3 data (Gaia Collaboration 2021; orange arrows in panel a) with our model (panel b). The proper motions of stars in the simulated NTA (panel (b) of Fig. 9) imply that they are moving towards the LMC, which matches well with *Gaia* results, except at the location closest of the LMC, for which model deviates from the observations. As in the observations, the dispersion of the proper motions in the simulated NTA are small. The length scale of proper motion vectors are different between model and observations data because of the lack of information about the amplitude of the observed proper motion vector (Gaia Collaboration 2021).

With MagES (Cullinane et al. 2020) combined with Gaia EDR3 data, Cullinane et al. (2022a, 2022b) have selected members of Magellanic Cloulds with fitting a multidimensional Gaussian distribution to the LOS velocity and proper motion. There are 26 selected fields observed in the periphery of LMC as indicated by red circles in the panel (a) of Fig. 9. With these data, they have derived the proper motions for each field, which are shown by red arrows in the panel (b) of Fig. 9 for comparison with our modeled proper motion. The proper motion of simulated NTA show downwards motion close to LMC disc, while the observation data show bottom right toward motion. We note that the four red arrows in the outmost bottom left disc have very large vector length. This could be due either to a small number of stars available for measurements from MagES, or because they are associated with faint substructures (El Youssoufi et al. 2021; Cullinane et al. 2022b) which are not reproduced by current models.

With MagES, the LOS velocity for each field is also derived from the members stars, which are shown by coloured circles in the panel (c) of Fig. 9 for comparison with our modeled line-of-sight velocity map. The simulated LOS velocity field follows well that observed (coloured circles).

We note that there is a radial velocity gradient across SMC with increasing radial velocity toward LMC. With new spectroscopic data of ∼3000 RGB and complemented by literature spectroscopic measurement, De Leo et al. (2020) have identified a large-scale radial velocity gradient for SMC with increasing velocity toward the MB (see their fig. 7). To have a better comparison with observations, we have collected observation data of radial velocities in the SMC from literature, including ∼3000 RGB stars from Dobbie et al. (2014), and ∼2000 from Evans & Howarth (2008) with majority of OBA type stars, as well as data from De Leo et al. (2020). These observed radial velocities in the SMC are shown within the small coloured circles in the panel (c) of Fig. 9. Even though these observed data are focused on the central SMC, the observed velocity gradient matched well with modeled one, confirming that the Wang et al. (2019) velocity field in SMC follows the observational data.

4 DISCUSSION

Even though the MS has been discovered for about 50 yr, there is still no agreement about its origin, which from the literature could be either a gigantic tidal tail, or two ram-pressure tails trailing behind each of the two Clouds. Both origins are consistent with the fact that the MS is trailing behind the Clouds (Mathewson et al. 1974), and that the recent collision between the Clouds had formed the Bridge. However, the tantalizing amount of high precision data provided by *Gaia* and ground-based surveys that is now available, is probably sufficient to disentangle which mechanisms lead to the MS formation.

In the following, we do not discuss the LA formation, which can be either attributed to the Cloud interaction (Besla et al. 2012; Lucchini et al. 2020), or to dwarfs passing ahead of the Clouds, which have lost their gas at different locations explaining then the LA four arm behaviour (Hammer et al. 2015; Tepper-García et al. 2019; Wang et al. 2019; Lucchini et al. 2021). First, this is because forcing the LA to be of the same origin than the MS could lead to misleading results. Secondly, there are more evidences that the LMC is associated to dwarfs (Patel et al. 2020), and also that many MW dwarfs have a recent infall like the LMC (Hammer et al. 2021), which let plausible a formation of the four leading arms by passages of several leading gas-rich dwarfs.

Table 1 provides a list of the Magellanic System main properties, and describes the ability of four modeling to reproduce them. We have chosen to describe only models based on a first passage of the Clouds, which let us with the tidal models of Besla et al. (2012) and Lucchini et al. (2020, 2021), and with the 'ram-pressure plus collision' model of Wang et al. (2019). Here we do not compare the model of Hammer et al. (2015), because the Wang et al. (2019) model is its direct adaptation by just changing the GADGET2 by the GIZMO software, for a better accounting of the Kelvin–Helmholtz (KH) instabilities. Such instabilities have to be accounted to constraint the MW halo gas content from the MS actual length and distance, as well as to properly account for the ionized gas kinematically associated to the MS (Fox et al. 2014).

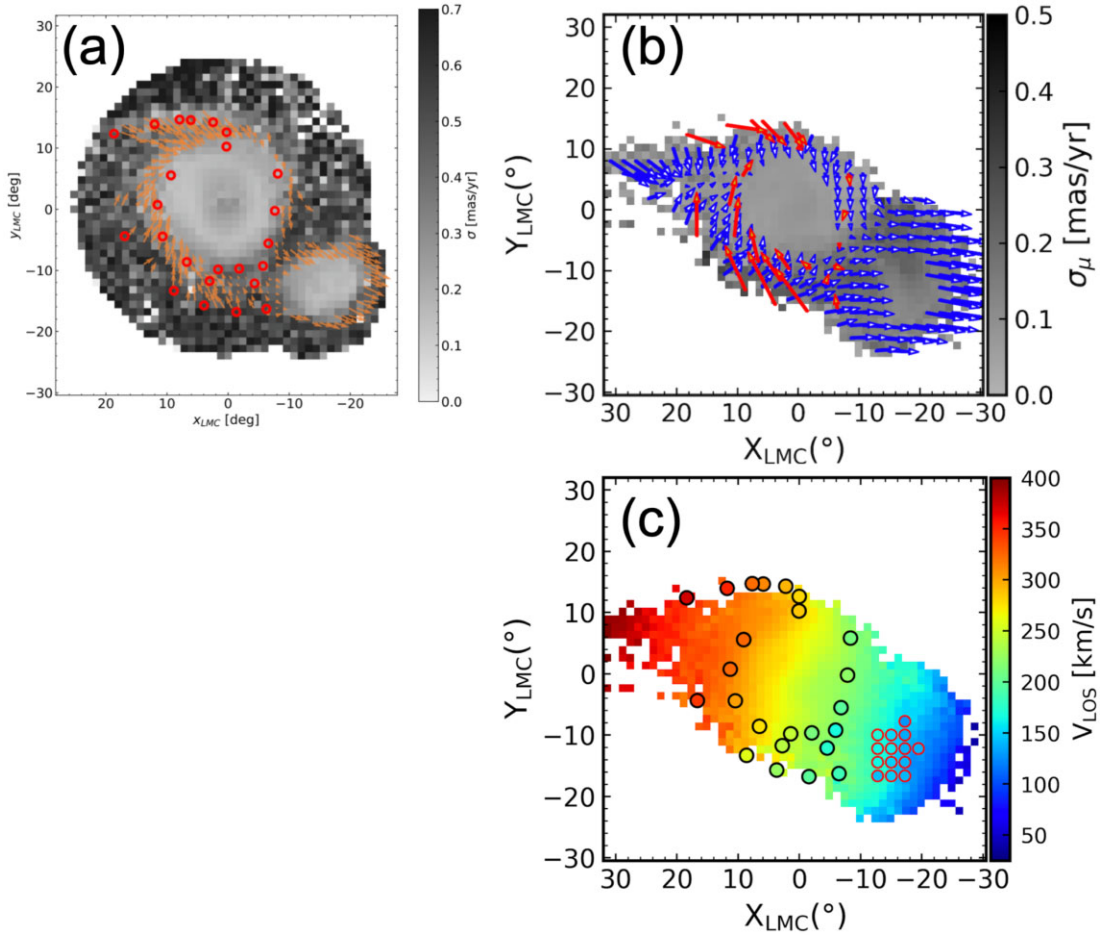

Figure 9. The panel (a) is from Gaia Collaboration (2021) with *Gaia* EDR3 showing the proper motion dispersion map and proper motion vectors shown by orange arrows. We note that there is no proper motion vector scale length available from Gaia Collaboration (2021). The red circles indicate the observed fields by MagES (Cullinane et al. 2020). The panel (b) shows the simulated MCs with blue arrows indicating the modeled proper motions, and the red arrows indicate the proper motions derived from MagES in each observed field. The panel (c) shows our modeled line-of-sight velocity field, and big coloured circles around LMC indicate the line-of-sight velocity from MagES (Cullinane et al. 2022a,b). The small coloured circles in the centre of the SMC are observed line-of-sight velocities from literature data (see the text for details).

Table 1. Comparing three modelings for reproducing the main properties of the Magellanic System.

Observation Constraints	Tidal Model Besla et al. (2012)	Ram-pressure + Collision Hammer et al. (2015) Wang et al. (2019)	Tidal + LMC corona Lucchini et al. (2020)	Tidal + LMC corona Lucchini et al. (2021)
MS ionized gas mass	N	Y	Y	N
MS ionized gas sky distribution	N	Y	Y	Y
MS H I total mass	N	Y	Y	Y
MS H I gas velocity distribution	Y	Y	N	Y
two inter-twisting filaments	N	Y	N	N
No stars in the MS	N	Y	N	N
Cloud proper motions	Y	Y	Y	N
H I bridge	Y	Y	Y	Y
Young and old stellar bridge	Y	Y	?	?

Ionized gas properties cannot be simulated by the Besla et al. (2012) model, since it does not include the MW halo gas, which cannot then interact with the predicted gaseous tidal tail. Because the Besla et al. (2012) model predicts a 10 times smaller H I mass than that observed in the MS is a major problem for this modeling, since adding the MW hot gas corona can only decrease the H I mass due to KH instabilities. However, this problem has been circumvented by Lucchini et al. (2020), who further added a hot corona to the LMC, in order to account for the large ionized gas mass associated to the MS.

In Table 1 we do not account for the mass properties of the remnant Clouds,[2] because these properties can be tuned after modifying

[2]Notice that the gas mass attached to the Clouds as well as the SMC shape are remarkably reproduced by Wang et al. (2019).

their initial conditions. However, the goal is to reproduce the whole MS properties, together with the Cloud orbital motions, for which measurements from *Gaia* accurately define their orbits and the way they have deposited their gas to form the MS.

Table 1 also shows that the Wang et al. (2019) model reproduces all the main properties of the MS, while other modeling fail for at least half of them. However, as argued by Tepper-García et al. (2019), one may consider that the initial conditions rely on a large number of model-dependent, and thus necessarily tuneable parameters leading to costly numerical experiments, and then prohibitive (or even 'futile') to explore in full the available parameter space. Following these considerations, one would only conclude that the 'ram-pressure plus collision' model is just the more advanced one by providing an explanation of all MS properties, but that a tidal model could in principle reach the same success.

However, this paper shows that the 'ram-pressure plus collision' model does not only reproduce the MS properties, but is also predictive, e.g. for the complex properties of stars in the Bridge, or for the NTA formation. Moreover, one may try to identify properties that cannot be reproduced by the tidal model. To do so, we propose to reinvestigate the physical properties of the MS as reported by Hammer et al. (2015) after their examination of the exquisite data from the Galactic All-Sky Survey (GASS; McClure-Griffiths et al. 2009; Kalberla et al. 2010). It revealed two inter-twisted filaments along the MS length, characterized by a transonic flow (see also Bland-Hawthorn et al. 2007) in a moderate to low turbulent medium (Reynolds parameter, R_e, of few hundred). These last properties are consistent with the presence of vortices anchored into the inter-twisted filaments (Hammer et al. 2015).

Perhaps the major drawback of the tidal model is that it cannot reproduce the MS morphology (e.g. the inter-twisted filament behaviour), including the fact that kinematic and chemical analyses indicate that gas from both the LMC and SMC is present in the MS, as it is argued by Lucchini et al. (2020). The Lucchini et al. (2020) simulations indeed include an additional filament that seems attached to the LMC as it is observed (Nidever, Majewski & Butler Burton 2008), but the simulated MS H I morphology is so wide (see their Fig. 2) that it shows very few similarities with the observed narrow inter-twisted filaments (see their fig. 2 Hammer et al. 2015). The major addition made by Lucchini et al. (2020) to the Besla et al. (2012) model from which it is adapted is indeed to add a Galactic corona to the MW as well as another corona to the LMC. The advantage of the later addition is to reproduce by construction the large amounts of ionized gas following the MS. However, this is at the cost of predicting a larger mass for the hot corona associated to the LMC than that linked to the MW (3×10^9 M$_\odot$ versus 2×10^9 M$_\odot$, respectively), which appears unrealistic.

Such a major difficulty has been identified and corrected by Lucchini et al. (2021), but at the cost of changing dramatically the Cloud orbits, in such a way that their accurately observed velocities are not reproduced at $\geq 3\sigma$ (and from 7σ to 18σ) for the LMC (SMC) tangential velocity components,[3] respectively. Fig. 10 shows the comparison of the 'ram-pressure plus collision' model (panel c and d) with observational data (panel a and b), the model is from

[3]In the notes to their table 1, Lucchini et al. (2021) quoted that due to numerical resolution they found extremely large uncertainties (up to 0.5 mas yr^{-1}) in their simulated proper motions, a problem that surprisingly seems to occur only in the tangential direction, and which we never encountered in Hammer et al. (2015) or in Wang et al. (2019) simulations.

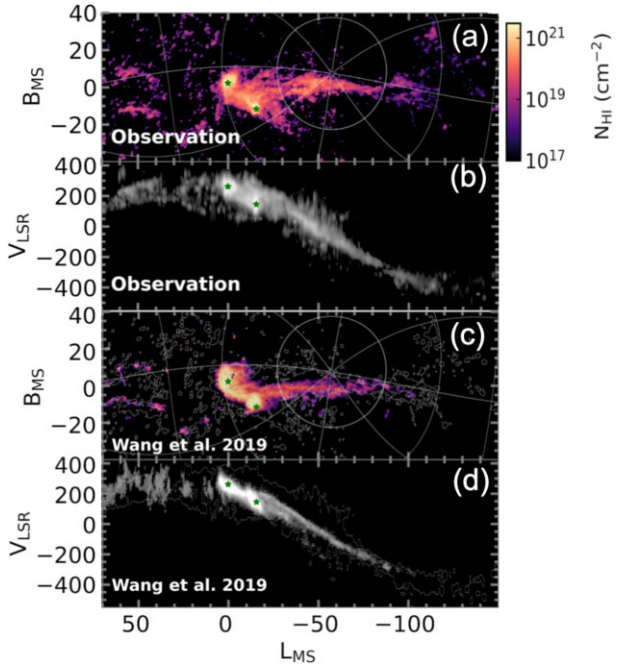

Figure 10. Comparison of MS in the distribution of Magellanic longitude versus latitude coordinates and longitude versus line-of-sight velocity. Panel (a) and (b) show the observation results from Nidever et al. (2010). The panel (c) and (d) show model results from the 'ram-pressure plus collision' model (Wang et al. 2019), assuming Leading Arm formation from Hammer et al. (2015) with a scenario of gas deposited from several former leading gas-rich dwarfs. The observations and model can be compared with the panel (d) and (e) of Fig. 3 of Lucchini, D'Onghia & Fox (2021), and the panel (b) and (c) of Fig. 2 of Lucchini et al. (2020) from tidal model with massive LMC corona.

Wang et al. (2019). In panels (c) and (d), the Leading Arm data from Hammer et al. (2015) have been added assuming the scenario of gas deposited from former runners of several gas-rich dwarfs. The model and observations can be compared with Fig. 2 in Lucchini et al. (2020) and Fig. 3 in Lucchini, D'Onghia & Fox (2021).

In summary, the 'ram-pressure plus collision' model succeeds to reproduce all the MS properties and is found to be also predictive, while the tidal model appears unable by construction to reproduce the very well defined inter-twisted filaments that constitute the MS. Moreover, tidal models that may reproduce the associated large amounts of ionized gas have led to inconsistencies either on the relative mass of the LMC versus MW coronas, or on the LMC and SMC tangential velocities.

Table 1 points out the fact that the 'ram-pressure plus collision' model naturally reproduce as much as possible the numerous properties of the Magellanic System. This could be considered as natural, since the LMC H I disc has been undoubtedly shrunk by ram-pressure effects (Nidever 2014), and such a gas is expected to be trailing to form the LMC contribution to the MS. The predictive ability of this model (MB population and NTA) further indicates that this model goes into the right direction to disentangle the mystery of Magellanic System formation (Mathewson, private communication). The only possible 'caveat' of the 'ram-pressure plus collision' model is that it predicts a moderate LMC mass to let the H I gas being extracted by ram-pressure to form the neutral Stream, especially between the Bridge and the tip-end. Wang et al. (2019) simulations are based on small masses for the LMC, and they mentioned having failed in reproducing the MS for LMC masses larger than 2×10^{10} M$_\odot$. In fact, the more massive is the ram-pressurized galaxy, the more

difficult is it to extract neutral H I gas (Yang et al. 2022). However, a full numerical study is needed to estimate the highest mass for the LMC halo that would not prevent the formation of the H I Magellanic Stream.

5 CONCLUSION

Here we show that the 'ram-pressure plus collision' model (Hammer et al. 2015; Wang et al. 2019) is able to reproduce all the MS properties, as well as to predict new features that have been observed after the model elaboration, without fine tuning. The new observation features include the complexity of the stellar populations in the MB and the NTA. The MB is likely caused by the Cloud collision 200–300 Myr ago, for which the LMC has tidally extracted large amounts of gas from the SMC, the MB gas being then affected by the ram-pressure exerted by the MW corona. Wang et al. (2019) explained as such the spatial and kinematic behaviour of both Young Main Sequence stars and ancient RR Lyrae stars (Belokurov et al. 2017). Besides this, the stellar populations found at two different distances in the MB region by Omkumar et al. (2021) are also predicted by the Wang et al. (2019) model. The model also predicts that the foreground population results from the Cloud tidal interaction (mostly stars extracted from the SMC), while the background population is associated to SMC spheroid stars that have been tidally extracted and reshaped by the LMC. We have also compared proper motions from *Gaia* EDR3 (Gaia Collaboration 2021) between young stars and the RC old stars in the MB region with Wang et al. (2019) model predictions. Both observations and model show that stars in the Bridge are moving consistently to the LMC. Recent identifications of the NTA and of its kinematics from *Gaia* EDR3 have been also reproduced by Wang et al. (2019) model, which infers its origin from the LMC tidal stretching by MW tidal force.

The ability of the 'ram-pressure plus collision' model contrasts with that of the tidal model that essentially fail to reproduce half of the main properties of the MS. In particular, the H I MS is mostly made of two inter-twisted filaments, which tidal models fail to reproduce, and for which no interpretation can be foreseen if the MS is a tidal tail. Moreover, the tidal model has difficulties to reproduce the MS gas mass, especially its dominant phase, the ionized gas, for which the proposed solutions appear either unrealistic, or with strong deviations from the calculated Cloud velocities. It is then likely that the MS is made by ram-pressure exerted by the MW corona to the Clouds since their entrance into the halo. This, combined with the 200–300 Myr collision that is robustly determined from the *Gaia* proper motions of the Clouds, from their common star formation history, and from the Bridge, suffices to explain the whole MS properties. We further conjecture that to form the Magellanic Stream, the LMC mass has to be smaller than 2×10^{10} $M_{\odot}$, though further studies are needed to precise the exact mass range.

ACKNOWLEDGEMENTS

We thank the referee for his/her helpful and insight comments, which help to improve the manuscript. The computing task was carried out on the HPC cluster at China National Astronomical Data Center (NADC). NADC is a National Science and Technology Innovation Base hosted at National Astronomical Observatories, Chinese Academy of Sciences. This work is supported by Grant No. 12073047 of the National Natural Science Foundation of China. We are grateful for the support of the International Research Program Tianguan, which is an agreement between the CNRS in France, NAOC, IHEP, and the Yunnan Univ. in China.

DATA AVAILABILITY

The data underlying this article will be shared on reasonable request to the corresponding author.

REFERENCES

Bagheri G., Cioni M.-R. L., Napiwotzki R., 2013, A&A, 551, A78
Belokurov V. A., Erkal D., 2019, MNRAS, 482, L9
Belokurov V., Erkal D., Deason A. J., Koposov S. E., De Angeli F., Evans D. W., Fraternali F., Mackey D., 2017, MNRAS, 466, 4711
Besla G., Kallivayalil N., Hernquist L., Robertson B., Cox T. J., van der Marel R. P., Alcock C., 2007, ApJ, 668, 949
Besla G., Kallivayalil N., Hernquist L., van der Marel R. P., Cox T. J., Kereš D., 2012, MNRAS, 421, 2109
Besla G., Hernquist L., Loeb A., 2013, MNRAS, 428, 2342
Bland-Hawthorn J., Sutherland R., Agertz O., Moore B., 2007, ApJ, 670, L109
Bregman J. N., Anderson M. E., Miller M. J., Hodges-Kluck E., Dai X., Li J.-T., Li Y., Qu Z., 2018, ApJ, 862, 3
Casetti-Dinescu D. I., Vieira K., Girard T. M., van Altena W. F., 2012, ApJ, 753, 123
Conroy C., Naidu R. P., Garavito-Camargo N., Besla G., Zaritsky D., Bonaca A., Johnson B. D., 2021, Nature, 592, 534
Cullinane L. R. et al., 2020, MNRAS, 497, 3055
Cullinane L. R., Mackey A. D., Da Costa G. S., Erkal D., Koposov S. E., Belokurov V., 2022a, MNRAS, 510, 445
Cullinane L. R., Mackey A. D., Da Costa G. S., Erkal D., Koposov S. E., Belokurov V., 2022b, MNRAS, 512, 4798
De Leo M., Carrera R., Noël N. E. D., Read J. I., Erkal D., Gallart C., 2020, MNRAS, 495, 98
Dehnen W., 1993, MNRAS, 265, 250
Demers S., Battinelli P., 1998, AJ, 115, 154
Dobbie P. D., Cole A. A., Subramaniam A., Keller S., 2014, MNRAS, 442, 1663
El Youssoufi D. et al., 2021, MNRAS, 505, 2020
Erkal D. et al., 2019, MNRAS, 487, 2685
Erkal D. et al., 2021, MNRAS, 506, 2677
Evans C. J., Howarth I. D., 2008, MNRAS, 386, 826
Faerman Y., Sternberg A., McKee C. F., 2017, ApJ, 835, 52
Fox A. J. et al., 2014, ApJ, 787, 147
Gaia Collaboration, 2021, A&A, 649, A7
Gatto M., Ripepi V., Bellazzini M., Tortora C., Tosi M., Cignoni M., Longo G., 2022, ApJ, 931, 19
Grady J., Belokurov V., Evans N. W., 2021, ApJ, 909, 150
Hammer F., Yang Y. B., Flores H., Puech M., Fouquet S., 2015, ApJ, 813, 110
Hammer F., Wang J., Pawlowski M. S., Yang Y., Bonifacio P., Li H., Babusiaux C., Arenou F., 2021, ApJ, 922, 93
Hopkins P. F., 2015, MNRAS, 450, 53
Irwin M. J., Kunkel W. E., Demers S., 1985, Nature, 318, 160
James D. et al., 2021, MNRAS, 508, 5854
Kalberla P. M. W., Haud U., 2006, A&A, 455, 481
Kalberla P. M. W. et al., 2010, A&A, 521, A17
Kallivayalil N., van der Marel R. P., Alcock C., Axelrod T., Cook K. H., Drake A. J., Geha M., 2006, ApJ, 638, 772
Kallivayalil N., van der Marel R. P., Besla G., Anderson J., Alcock C., 2013, ApJ, 764, 161
Lucchini S., D'Onghia E., Fox A. J., Bustard C., Bland-Hawthorn J., Zweibel E., 2020, Nature, 585, 203
Lucchini S., D'Onghia E., Fox A. J., 2021, ApJ, 921, L36
McClure-Griffiths N. M. et al., 2009, ApJS, 181, 398
Mackey A. D., Koposov S. E., Erkal D., Belokurov V., Da Costa G. S., Gómez F. A., 2016, MNRAS, 459, 239

Mackey D., Koposov S., Da Costa G., Belokurov V., Erkal D., Kuzma P., 2018, ApJ, 858, L21
Mastropietro C., 2010, in Debattista V. P., Popescu C. C., eds, AIP Conf. Ser. Vol. 1240, Hunting for the Dark: the Hidden Side of Galaxy Formation. Am. Inst. Phys., New York, p. 150
Mathewson D., 2012, J. Astron. His. Heritage, 15, 100
Mathewson D. S., Cleary M. N., Murray J. D., 1974, ApJ, 190, 291
Miller M. J., Bregman J. N., 2013, ApJ, 770, 118
Muraveva T. et al., 2018, MNRAS, 473, 3131
Nidever D. L., 2014, in Seigar M. S., Treuthardt P., eds, ASP Conf. Ser. Vol. 480, Structure and Dynamics of Disk Galaxies. Astron. Soc. Pac., San Francisco, p. 27
Nidever D. L., Majewski S. R., Butler Burton W., 2008, ApJ, 679, 432
Nidever D. L., Majewski S. R., Butler Burton W., Nigra L., 2010, ApJ, 723, 1618
Nidever D. L. et al., 2013, in American Astronomical Society Meeting Abstracts, Vol. 221. p. 404.04
Noël N. E. D., Conn B. C., Carrera R., Read J. I., Rix H.-W., Dolphin A., 2013, ApJ, 768, 109
Omkumar A. O. et al., 2021, MNRAS, 500, 2757
Patel E. et al., 2020, ApJ, 893, 121
Piatek S., Pryor C., Olszewski E. W., 2008, AJ, 135, 1024
Richter P. et al., 2017, A&A, 607, A48
Ripepi V. et al., 2017, MNRAS, 472, 808
Schmidt T. et al., 2020, A&A, 641, A134
Scowcroft V., Freedman W. L., Madore B. F., Monson A., Persson S. E., Rich J., Seibert M., Rigby J. R., 2016, ApJ, 816, 49
Skowron D. M. et al., 2014, ApJ, 795, 108
Tepper-García T., Bland-Hawthorn J., Pawlowski M. S., Fritz T. K., 2019, MNRAS, 488, 918
van der Marel R. P., Kallivayalil N., 2014, ApJ, 781, 121
Vasiliev E., Belokurov V., Erkal D., 2021, MNRAS, 501, 2279
Wang J., Hammer F., Yang Y., Ripepi V., Cioni M.-R. L., Puech M., Flores H., 2019, MNRAS, 486, 5907
Yang Y., Ianjamasimanana R., Hammer F., Higgs C., Namumba B., Carignan C., Józsa G. I. G., McConnachie A. W., 2022, A&A, 660, L11
Zaritsky D. et al., 2020, ApJ, 905, L3
Zheng Y., Putman M. E., Peek J. E. G., Joung M. R., 2015, ApJ, 807, 103
Zheng Y., Peek J. E. G., Putman M. E., Werk J. K., 2019, ApJ, 871, 35
Zivick P. et al., 2018, ApJ, 864, 55
Zivick P. et al., 2019, ApJ, 874, 78

APPENDIX A: GAUSSIAN FITTING TO THE DISTANCE DISTRIBUTION

Two Gaussian function are used to fit the distance distribution of particles within different MB longitude bins as shown in Fig. A1.

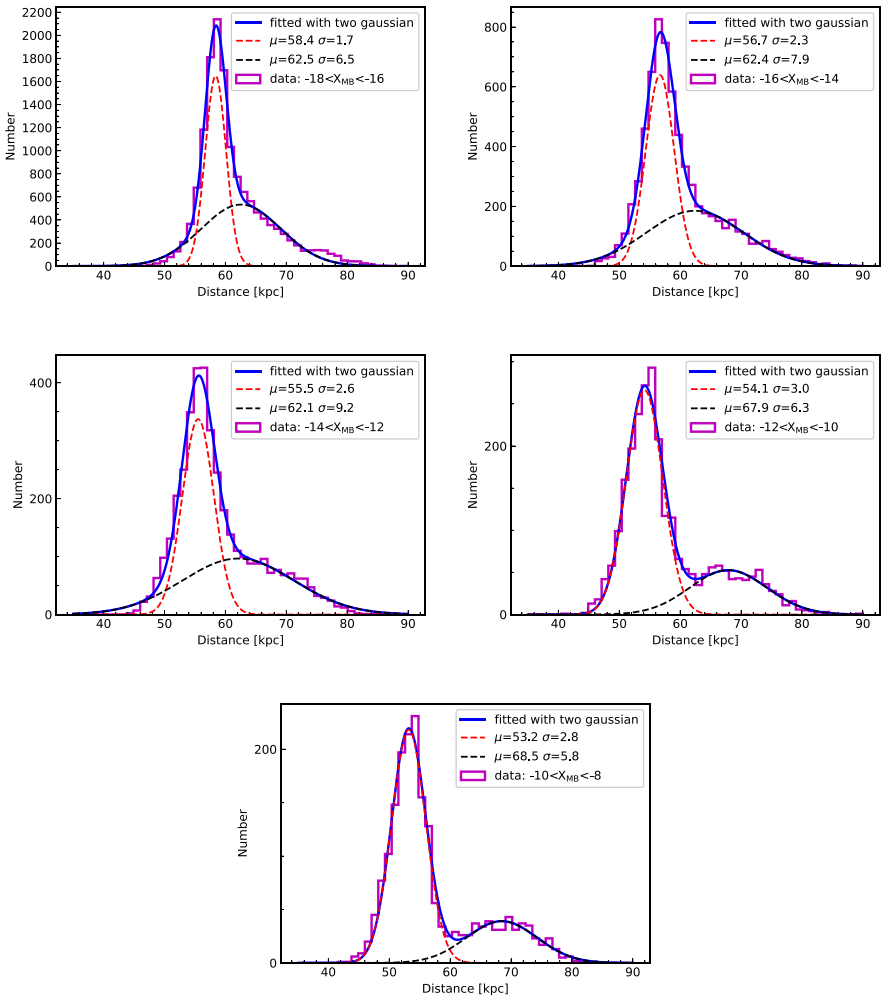

Figure A1. Distances distributions for particles (magenta) within different MB longitudes intervals. Two Gaussian functions are used to fit the distance distributions for foreground (red-dashed line) and background (black-dashed line) population, with their mean and standard deviation are labeled on the top right of each panel. The blue-solid line indicate the sum of two Gaussian functions.

This paper has been typeset from a TEX/LATEX file prepared by the author.